

ORIGINAL RESEARCH ARTICLE

A cost-effective method for estimating long-term effects of waves on beach erosion with application to Sitia Bay, Crete

Flora E. Karathanasi^{a,b,*}, Kostas A. Belibassakis^a

^a School of Naval Architecture & Marine Engineering, National Technical University of Athens, Athens, Greece

^b Institute of Oceanography, Hellenic Centre for Marine Research, Anavyssos, Greece

Received 24 July 2018; accepted 5 December 2018

Available online 19 December 2018

KEYWORDS

Beach erosion;
Bed level evolution;
Wave/current
modelling;
Shields criterion;
Sitia-Crete coast

Summary Considering the significant role of beaches for the sea environment and welfare of coastal communities, a variety of process-based models are applied in order to examine and understand the interaction of hydrodynamic processes with seabed material at different time scales. However, a long-term view of this interaction requires a great amount of computational time. In this work a cost-effective methodology is proposed to surpass this shortcoming and estimate bed level evolution. The technique is relied on an objective criterion to assess spectral wave time series of wave height, period and direction and identify the wave conditions that contribute to the initiation of sediment movement. After implementing the so-called Shields criterion, the full wave climate is reduced to two classes of representative wave conditions: the over-critical ones, mainly responsible for long-term erosion, and the sub-critical wave conditions. By applying a well-known process-based model, the representative wave conditions are used as input for the wave-current-sediment transport simulation and rates of bed level changes are obtained, on the basis of which the long-term effects of waves on beach erosion are estimated. Taking into account that erosion is a threatening phenomenon along the sandy beaches of Mediterranean Sea, the present method is demonstrated at a sandy coast of Sitia Bay, Crete. The bed levels derived from the proposed methodology and the full time series are compared. The results indicate reasonable agreement at the selected locations with deviations under 7%, and conformity of the tendency of seabed evolution, rendering the new methodology a useful tool. © 2018 Institute of Oceanology of the Polish Academy of Sciences. Production and hosting by Elsevier Sp. z o.o. This is an open access article under the CC BY-NC-ND license (<http://creativecommons.org/licenses/by-nc-nd/4.0/>).

* Corresponding author at: School of Naval Architecture and Marine Engineering, National Technical University of Athens, Zografos 15773, Athens, Greece. Tel.: +30 210 7721103

E-mail address: flora@mail.ntua.gr (F.E. Karathanasi).

Peer review under the responsibility of Institute of Oceanology of the Polish Academy of Sciences.



Production and hosting by Elsevier

<https://doi.org/10.1016/j.oceano.2018.12.001>

0078-3234/© 2018 Institute of Oceanology of the Polish Academy of Sciences. Production and hosting by Elsevier Sp. z o.o. This is an open access article under the CC BY-NC-ND license (<http://creativecommons.org/licenses/by-nc-nd/4.0/>).

1. Introduction

Understanding erosion and accretion processes in a coastal area and accurately forecasting coastal evolution is essential in order to prioritize mitigation measures and manage planning decisions and prospective interventions as regards the protection of the coastal environment and its sustainable development. Numerous scientific studies have been conducted over the past decades dealing with coastal erosion and morphological changes; see, for instance, the recent review papers on coastal erosion under climate change scenarios by [Ranasinghe \(2016\)](#) and [Toimil et al. \(2017\)](#). Nevertheless, it is yet a challenging field of research since the sufficient and proper understanding of the underlying processes and dynamics is still lacking due to the complex and non-linear interactions of the involved processes; see, e.g. [Davidson-Arnott \(2009\)](#).

Process-based models have been widely used to simulate morphological processes and estimate sediment transport rates and bathymetry evolution for different time scales during recent years. Such models are based on mathematical formulation and assumptions in order to assess sediment transport processes, and are ideal for short-term simulations (hours to weeks); however, for medium- and long-term processes, they suffer from inherent constraints such as the high computational time, sensitivity to initial conditions and numerical instabilities. Some relevant and recent studies based on process-based models are the works of [Ramakrishnan et al. \(2018\)](#), who simulated morphological changes under normal wave conditions and storm events during a four-month period along a pocket beach at the east coast of India, of [Dubarbier et al. \(2015\)](#), who simulated beach profile evolution on the timescales from hours to months encompassing both slow onshore and rapid offshore sandbar migration events at two sites, and of [Corbella and Stretch \(2012\)](#), who examined the impacts of decadal trends on storm induced beach erosion based on a non-stationary multivariate statistical model combined with three process-based models.

In order to reduce computational time that is required for simulations of morphological models with time period of one year or greater, retaining an acceptable accuracy of the predictions, wave input reduction methods have been suggested. The core idea of these techniques is to reduce the size of the wave input data at a coastal area of interest with some sets of representative wave conditions based on specific criteria. A detailed analysis of five techniques dealing with input reduction has been performed by [Benedet et al. \(2016\)](#). In that study, one-year reference wave data representing the full wave climate at a south-east coast of Florida, USA, were transformed to four different numbers of representative wave conditions. Specifically, the full wave climate was reduced to 30, 20, 12 and 6 representative wave cases in order to run the corresponding models in sequence for a smaller time period; these numbers were selected based on sensitivity tests carried out by the authors. According to the frequency of occurrence of each wave condition in a full year, the sediment transport patterns were estimated for each proposed technique along with the simulation of the detailed wave climate, used as benchmark. The results obtained by each technique were compared with the corresponding results of the benchmark in terms of root mean square error.

The analysis showed that for a small number of wave conditions (i.e. 12 and 6) the method with the best performance is the “Energy Flux Method”, where directional bins of equal wave energy flux were formed; on the other hand, as the size of representative wave cases was increasing, all methods had a similar performance. Furthermore, [Walstra et al. \(2013\)](#) introduced an input reduction method at two wave-dominated coasts with dissimilar long-term offshore wave direction characteristics. Their analysis also demonstrated that apart from storm events, which contribute to the largest morphological changes, it is essential to preserve in the reduced wave climate the wave energy conditions with low or intermediate intensity for a more realistic long-term sandbar behaviour.

The same rationale is also adopted when examining coastal erosion in terms of wave action, where there are two main viewpoints. The first one refers to the episodic events (e.g. storms, tsunamis) that act for a short time window (hours to some days) but can cause significant and sudden damages, from loss of land and destruction of coastal infrastructure to direct impacts on coastal communities and the adjacent coastal ecosystems, among others. The second one deals with the accumulative wave action, where erosion behaviour is governed by the interaction of storm events and calm periods. In a previous work by the authors ([Belibassakis and Karathanasi, 2017](#)), the first viewpoint was examined with application to the Varkiza coast in the Saronic Gulf (western Aegean Sea); the present study focuses on the second viewpoint. To this end, in this work a cost-effective method is introduced based on the use of process-based models combined with the philosophy of wave input reduction techniques. The proposed technique relies wave input reduction on a grain motion initiation criterion in terms of orbital velocity, from which two basic categories are separated: (i) the one dealing with wave conditions that contribute to the wave-induced initiation of sediment movement at depths around the closure depth, and (ii) the other one including the low energetic wave conditions. Other reference works as regards the onset of sediment motion under waves are those of [Hallermeier \(1980\)](#), [Soulsby \(1997\)](#), and [Van Rijn \(1993\)](#). Consequently, the computational efficiency of estimating bed level can be drastically increased with the proposed methodology instead of using the full wave time series, while the accuracy level can be retained into acceptable limits.

As an application the coast of Sitia, in the eastern part of Crete Isl., is examined as a specific case study. The main reasons for selecting this particular coast lie in its vulnerability to erosion phenomena and its touristic character; see [Fig. 1\(a\)](#). Specifically, a recent study ([Alexandrakis et al., 2015](#)) based on aerial photographs between 1945 and 2014, indicated that the coastline has been retreated for a distance of the order of 45 m (representing the maximum value) while in [Foteinis and Synolakis \(2015\)](#), the mean coastal retreat rate at Sitia was estimated at 0.32 m/yr, among the highest erosion rates in Crete, utilizing aerial photographs (1960–2004), satellite images (2003–2012) and field survey measurements (2009–2012). Indicatively, aerial and satellite images from Google Earth show that 7 m is the maximum loss during the period 2002–2015; see also [Fig. 1\(b\)](#). In 2016, the collapse of the retaining wall of the coastal road brought the erosion matter to a climax leaving some villages in the

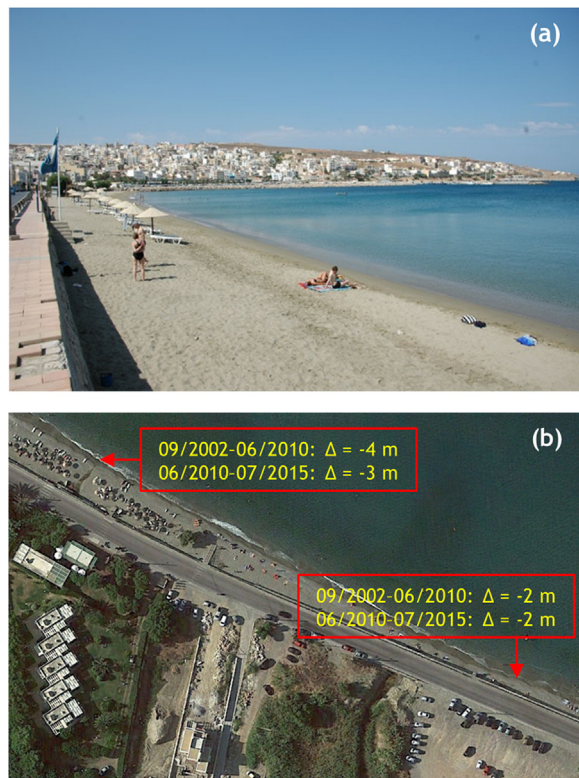


Figure 1 (a) Western part of the beach at Sitia Bay. (b) Coastline retreat at the central part.

north-eastern part inaccessible until the end of repair works. However, from Google Earth images, it seems that in 2017 there was a widening along the beach, which can be attributed to natural processes since no beach nourishment took place. Additionally, the touristic activities in the wider area have become more intensive the last years rendering confronting, prediction and management of erosion even more imperative. A preliminary study as regards the sediment transport patterns under two alternative wave scenarios (i.e. mean sea state, harsh wave conditions that contribute to initiation of sediment motion) and three different topographies of the seabed (i.e. current state, two submerged breakwaters at the isobaths of 5 m, port extension in the sea) has been conducted by the same authors at the same study area (Karathanasi et al., 2017). One of the main conclusions of this study as regards the harsh wave conditions for all the examined seabed topographies was the clockwise current circulation that contributed to the sediment movement westward.

Since the availability of in situ wave measurements from oceanographic buoys is rather limited in space and time, the analysis is based on statistical parameters, like significant wave height and peak period, derived from wave models that are quickly accessed nowadays. Thereupon, in this study time series of wave statistical parameters are derived from the Mediterranean Sea Waves forecast system, which is based on the third-generation wave model WAM Cycle 4.5.4 (Günther and Behrens, 2012). Moreover, current velocity time series are obtained from the Med-currents system, whose equations are solved by an Ocean General Circulation Model based on

the NEMO model (version 3.6); for more details, see Clementi et al. (2017). Both datasets can be accessed at <http://marine.copernicus.eu/services-portfolio/access-to-products/>. The process-based numerical model used for the detailed description of currents, waves, sediment transport and bed level update and their interdependence is the MIKE 21 Coupled Model FM (DHI, 2016). The same numerical wave model has been applied in relevant recent studies; see, e.g. Aouiche et al. (2016), Belibassakis and Karathanasi (2017), Daghigh et al. (2017), Gad et al. (2018), and Gharibreza et al. (2018).

The structure of the present paper is as follows: in Section 2, the proposed methodology is presented, which provides the bed level for a specified time period, after appropriately reducing the available wave time series. A detailed description of the study area is given in Section 3 and an overview of the model setup, including the bathymetry of the model domain, the analyzed wave climate and the input data for the various modules can be found in Section 4. Subsequently, in Section 5, the results of this procedure are presented and compared with the results from the simulation of the full time series. Discussion and further comments are given in Section 6, and in the final section, the main findings of this work are summarized along with some suggestions for further research.

2. Methodology

When a long-term time series of wave data is available near-shore, the core of the proposed methodology is based on the rationale of wave input reduction. The wave conditions that contribute to the onset of sediment motion below the closure depth of a sandy bed level, called hereafter “over-critical wave conditions”, form the determinative factor of this analysis. With the term “closure depth”, we define the transition zone in which the influence of waves on bed stresses, and hence sediment transport, is significantly lower than within the region of wave breaking (i.e. surf zone) or the region where the effects of wave energy dissipation are dominant (i.e. upper shoreface zone) (Ortiz and Ashton, 2016). Hence the underlying assumption as regards closure depth is its dependence on the harsh wave conditions. In this context, it is possible to significantly reduce computation times and speed up the whole analysis. The proposed approach uses the wave statistical parameters such as significant wave height H_s and peak period T_p , along with some basic hydrodynamic parameters (e.g. wave height, sea water density) and sediment characteristics (e.g. d_{50} , density of sediment), to estimate bottom orbital velocity u_b and wave shear velocity u_{*w} , rendering the methodology fully applicable and handy, since in the majority of the cases such summary data are available (e.g. wave model outputs, archived wave data).

Before proceeding with the description of the methodology, for the sake of simplicity, let us first provide the appropriate definitions regarding the points used in the analysis that are mentioned in the subsequent sections:

- the offshore points that correspond to the available wave time series, forming the input for the boundary of the outer model domain with the coarse spatial resolution, are denoted by P_{out} ;

- the points that are used as input for the boundaries of the inner model domain with the fine spatial resolution, obtained after applying a wave transformation scheme, are denoted by P_{inn} , and the middle point of the northern boundary is denoted by $P_{inn,m}$;
- the point that represents the closure depth is denoted by P_{cd} , and the corresponding depth h_{cd} is defined by the [Hallermeier \(1981\)](#) equation given by:

$$h_{cd} = 2.28H_{eff} - 68.5 \left(\frac{H_{eff}^2}{gT_{eff}^2} \right), \quad (1)$$

where H_{eff} is the effective wave height, exceeded 12 h in a single year (i.e. the greatest 0.137% waves during a year) and T_{eff} is the associated wave period.

2.1. Description of the cost-effective method

According to linear wave theory, the bottom (or near-bed) orbital velocity of a monochromatic wave is related to water depth and surface wave conditions as follows:

$$u_b = \frac{\pi H}{T \sinh(kh)}, \quad (2)$$

where H is the wave height, T is the wave period and $k = 2\pi/\lambda$ is the wavenumber (λ is the wavelength) and h is the water depth. Eq. (2) is extended for multichromatic waves in the coastal environment by applying it for all frequencies of the wave spectrum corresponding to each sea state and summing the components. Thus, a representative bottom orbital velocity u_{br} is calculated; see, e.g. [Madsen \(1994\)](#). Following the method suggested by [Wiberg and Sherwood \(2008\)](#), a generic form of the wave spectrum is used to estimate bottom orbital velocity from the values of H_S and T_P of the reference wave data (i.e. the entire time series of the available wave data) at a point that represents the closure depth, denoted by P_{cd} . Among the commonly used wind-generated wave spectra, JONSWAP spectrum ([Hasselmann et al., 1973](#)) is adopted,

$$S_{\eta}(\omega) = B \left(\frac{H_S}{4} \right)^2 \frac{\omega_p^4}{\omega^5} \exp \left[-\frac{5}{4} \left(\frac{\omega}{\omega_p} \right)^{-4} \right] \gamma^{(\omega/\omega_p)}, \quad (3)$$

where $\omega_p = 2\pi/T_P$ is the peak angular frequency, $B = 3.29$, $\gamma = 3.3$ and $\phi(\omega/\omega_p) = \exp[-0.5\beta^{-2}(\omega/\omega_p - 1)^2]$ with $\beta = 0.07$ for $\omega \leq \omega_p$ and $\beta = 0.09$ for $\omega > \omega_p$.

The representative orbital velocity u_{br} is then calculated from the following relation

$$u_{br} = \sqrt{2 \left(\sum_i S_{u,i} \Delta\omega_i \right)}, \quad (4)$$

with $S_{u,i} = \frac{4\pi^2}{T_i^2 \sinh^2(k_i h)} S_{\eta,i}$.

For the sediment transport purposes, another important property of waves is the bed shear stress τ_{bw} that can be associated with u_b and a wave friction factor f_w by:

$$\tau_{bw} = \frac{1}{2} \rho_w f_w u_b^2, \quad (5)$$

where ρ_w is the sea water density. f_w is calculated by the following empirical relationship ([Fredsoe and Deigaard, 1992](#)):

$$f_w = \begin{cases} 0.04 \frac{\alpha^{-0.25}}{k}, & \frac{\alpha}{k} > 50 \\ 0.4 \frac{\alpha^{-0.75}}{k}, & \frac{\alpha}{k} < 50, \end{cases} \quad (6)$$

where $\alpha = 0.5H/\sinh(kh)$ is the wave orbital amplitude and k_N is the Nikuradse's bed roughness parameter equal to $2.5d_{50}$, where d_{50} is the median sediment grain diameter.

Wave shear velocity u_{*w} is defined as follows:

$$u_{*w} = \sqrt{\frac{\tau_{bw}}{\rho_w}}. \quad (7)$$

The dimensionless bed shear stress, i.e. the Shields parameter θ^* , defined as

$$\theta^* = \frac{u_{*w}^2}{(s-1)gd_{50}}, \quad (8)$$

with $s = \rho_s/\rho_w$ denoting the ratio between the density of bed material and sea water (ρ_s is the density of the sediment) and g denoting the acceleration caused by gravity (9.81 m/s^2), is used to indicate the lower threshold value for initiation of sediment motion for the cases that $\theta^* > \theta_{cr}$, where $\theta_{cr} = 0.045$ is the critical bed shear stress.

Based on the above threshold value of initiation of sediment movement, the proposed methodology can be applied on the available wave time series at P_{cd} in order to indicate the specific timesteps that represent these wave conditions yielding a value of θ^* higher than 0.045 (i.e. over-critical wave conditions). Let us note that in case the available wave time series is available at an offshore location, like P_{out} points, a wave transformation process should be necessarily implemented in order to obtain the corresponding time series at the closure depth. Having these over-critical wave conditions at P_{cd} to hand, the corresponding conditions at the boundary of the inner model need to be extracted, represented by $P_{inn,m}$. Since the temporal resolution of the wave time series is 1 hour and given the distance between the offshore boundary (of the inner model) and P_{cd} ($\sim 1.6 \text{ km}$), the over-critical wave conditions at the boundary of the inner model that contribute to the initiation of sediment motion are identified based on the same timestep that gives each over-critical wave condition at P_{cd} . Then, these over-critical conditions are classified at $P_{inn,m}$ into specific intervals of H_S and T_P (0.5 m and 1 s, respectively) with equidistant binning (i.e. constant bin-size) and the corresponding mean wave direction θ_m is calculated for each class. This schematization (into (H_S, T_P, θ_m) triplets) is essential in order to proceed with the proposed methodology described in detail in the remaining part of this section.

Apart from the over-critical wave conditions, in which the morphological changes are large, the conditions where wave-induced currents are dominant should be additionally considered for a more realistic long-term behaviour of bed level. Assuming that waves below 0.5 m at the boundary of the inner model do not produce significant erosion/accretion patterns in the shore, the calm wave climate, called hereafter “sub-critical wave conditions”, is grossly classified for values of H_S smaller than the threshold values and higher than 0.5 m. In this case, the intervals for H_S remain 0.5 m and for T_P the interval is varying (from 1 s to 4 s). The corresponding mean wave directions θ_m for the selected pairs (H_S, T_P) is also calculated.

The final triplets of both the over- and sub-critical wave conditions comprise the input for MIKE 21 Coupled Model Flexible Mesh (called hereafter MIKE21 CFM) simulations, which is the process-based model used in this work; see also Sections 4 and 5. From these simulations the rate of bed level change q is extracted for a 2-week simulation period with 1-hour timestep. This time period allows a detailed sediment response for the specific triplets and a more accurate estimation of a mean rate q . Let us note that the rates estimated for the over- and sub-critical wave conditions are appropriately weighted based on the frequency of occurrence of each selected class.

After the schematization of the over- and sub-critical wave conditions, from the simulation results, the rate of bed level change is estimated based on the sediment continuity equation. The mean rate of bed level change q [m/day] for each triplet is calculated by

$$a = \frac{\sum_{i=2}^n q_i}{n-1}, \tag{9}$$

where n is the total number of timesteps during the 2-week simulation period. The rate of the first timestep q_1 is considered as an initialization rate of the simulations and for this reason, it is excluded from Eq. (9).

For the proposed methodology, the bed level is estimated by

$$h(jt) = h(jt-1) + q, \quad j = 1, \dots, n, \tag{10}$$

at the t th 1-hour interval for each (H_s, T_p, θ_m) triplet.

Based on the above mentioned description and definitions, the frame of the cost-effective methodology is presented in Fig. 2. Recapitulating the steps that should be followed for implementing the proposed methodology, the following key-aspects should be addressed:

1. Obtain wave time series at P_{inn} points and P_{cd} , if wave data are only available offshore;
2. Calculate bottom orbital velocity, wave shear velocity and bed shear stress at P_{cd} ;
3. If $\theta^* > \theta_{cr}$ at P_{cd} , then identify the corresponding values of H_s and T_p at P_{cd} . Based on the timestep of each pair, extract the corresponding over-critical values of (H_s, T_p) at $P_{inn,m}$. Then, group these pairs and calculate mean value of θ_m for each class;

4. If $\theta^* < \theta_{cr}$ at P_{cd} , then identify these values of H_s that are both higher than 0.5 m and different from the over-critical values (from step 3) along with the corresponding values of T_p . Then, group these pairs and calculate mean value of θ_m for each class;
5. Calculate the rates of bed level change with MIKE21 CFM for both over- and sub-critical values for each (H_s, T_p, θ_m) triplet;
6. Finally, calculate bed level at any location of the inner model domain via Eq. (10).

3. Study area

The area of interest is Sitia beach that is located in the north-eastern part of the Prefecture of Lassithi, Crete, on the west side of the homonymous bay; see Fig. 3. It is a 2-km long beach with variable width of maximum value around 35 m, and exhibits a typical U-shape in the NW-SE orientation. Due to the shape and orientation of the examined beach, the wave action is confined to the north and north-eastern directions, which is the primary factor for the settlement of sediments. At the western part of the beach there is a river system (Pantelis- or Stomios-river), following dry and wet periods, that discharges into the bay, and there is also the homonymous port that can accommodate both small fishing vessels and larger merchant and passenger vessels.

Fig. 3 also presents an overview of the points mentioned in Section 2 for the case study of this work. Let us note that in this case study $h_{cd} = 6.5$ m, thus P_{cd} was selected on the isobath of 6.5 m and in the middle of the longshore direction of the beach.

The homonym town, Sitia, has become a tourist attraction the last decades, mainly during the summer period, while tourist infrastructures (e.g. hotels, restaurants), and in general human activities, place pressure on the coastal environment. Moreover, the main road that connects Sitia with other tourist destinations at the eastern part of the island, such as the palm forest Vai, was developed to a great extent beside the coastal front.

To this end, erosion phenomena are evident due to both the intensive residential and infrastructure-based development of the wider area along with the physical conditions that seem to be more frequent and of longer duration.

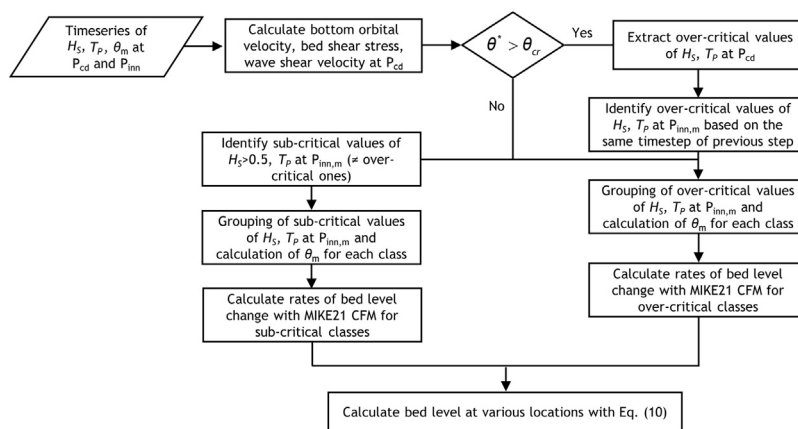


Figure 2 Flow chart of the proposed methodology.

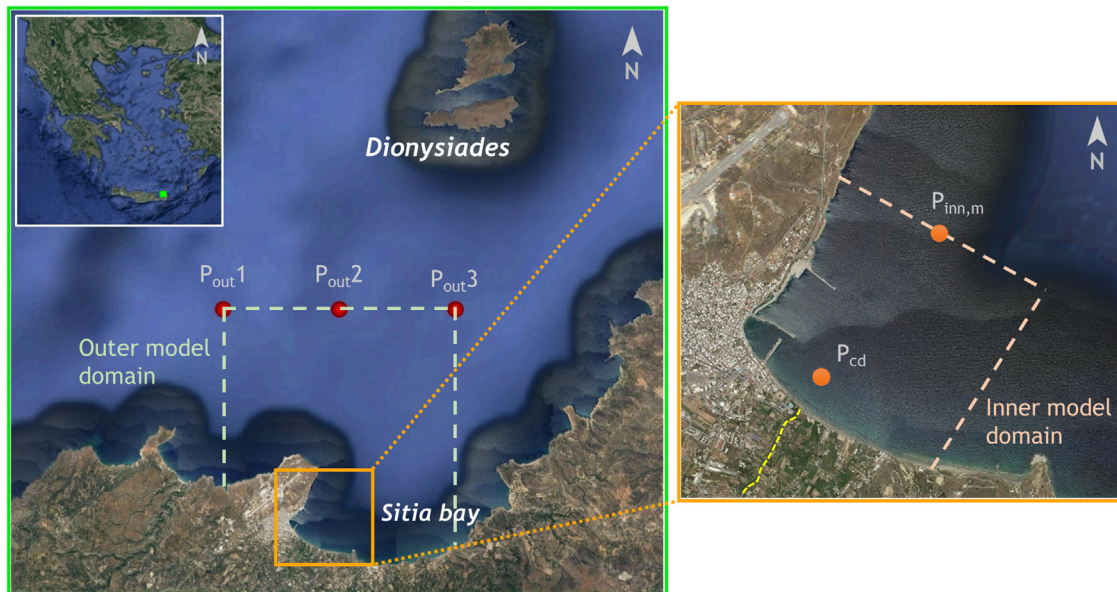


Figure 3 Aerial map of Sitia Bay along with the offshore locations of the input data for the outer model domain (left map), and the study area of Sitia beach (inner model domain) along with the locations of $P_{inn,m}$ and P_{cd} (right map) used in the analysis. Source: Google Earth.

Specifically, at the end of 2016 the front of the coastal road that is contiguous to the eastern part of the beach collapsed after the accumulative action of intense weather conditions that took place the last few years, causing several problems and safety issues to the local residents and tourists. Moreover, the sediment supply of the beach is relatively limited while the construction of the adjacent harbour at the western part of the coast, in order to serve the needs for tourism and fishing, puts additional pressures and intensifies erosion rates.

4. Model setup

As mentioned above, the process-based numerical model that is used in this study is MIKE21 CFM developed by the Danish Hydraulic Institute (DHI). MIKE21 CFM is a depth-averaged two-dimensional numerical model used to study and simulate a wide range of coastal hydrodynamic problems including the description and interaction of the relevant processes, such as currents, waves and sediment transport in coastal areas, among others. This numerical modelling software package includes several interrelated modules, of which the following are used for the purpose of this study: (i) the hydrodynamic (HD) module; (ii) the spectral wave (SW) module, and; (iii) the sand transport (ST) module. Through a dynamic coupling, hydrodynamic and spectral wave computations are performed simultaneously to calculate sediment transport rates and update bathymetry at each timestep. Specifically, sediment modelling is established on: (i) a depth-averaged hydrodynamic model, based on the depth-integrated incompressible Reynolds averaged Navier-Stokes equations; (ii) a phase-averaged wave model, based on the wave action conservation equation, and; (iii) sediment transport tables calculated in advance for every combination of current, wave, bathymetry and sediment conditions appear-

ing in the simulation; for a more detailed description of the three modules, see Belibassakis and Karathanasi (2017).

In the following subsections, the boundary conditions and the model parameters used for the model simulations are described for each module, along with some necessary information as regards the model grid and wave climate.

4.1. Bathymetry and unstructured grid

As already mentioned, in this analysis, the outer model domain is used for the transformation of the wave conditions from the available wave time series towards the shore. This model domain covers a distance of 7.5 km in the longshore direction and 7.8 km for the cross-shore one. The total number of triangular elements in the outer domain is 1,284 with 759 nodes while the maximum size of the elements is approximately 0.12 km^2 ; see also Fig. 4(a). The bathymetry of the outer model domain presented in Fig. 4 (b), shows that the seabed topography is quite mild. From the shoreline up to the isobath of -75 m , the contours are parallel and the maximum depth (-226 m) is observed at the north-western part of the domain.

As regards the inner model domain, it is divided into two nested grid domains, going gradually from the outer area with the lower resolution (i.e. level 1) up to the computational grid with the highest resolution (i.e. level 2), where the smaller triangular elements represent areas where the accuracy in the wave, current and sediment transport calculations are important; see also Fig. 5(a) for the representation of the different levels and the final mesh generation of the examined area. Specifically, level 1 extends both in the longshore and cross-shore directions approximately 1.7 km with the area of each triangular element not exceeding $6,580 \text{ m}^2$. Let us note in advance that the appropriate forces are imposed at the boundaries of the outmost level (i.e. level 1) for the generation of

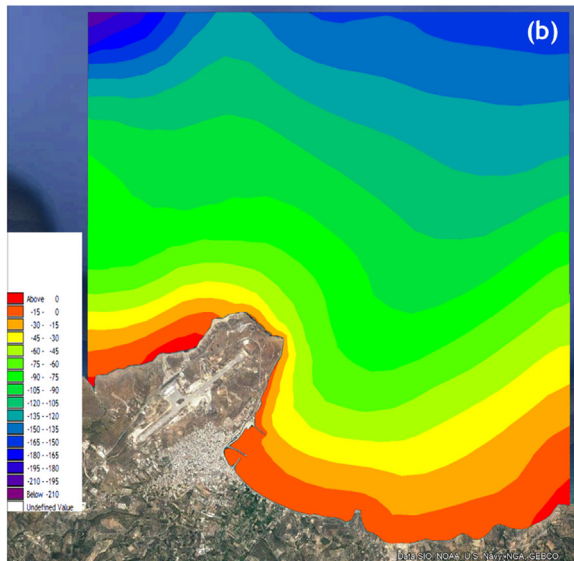
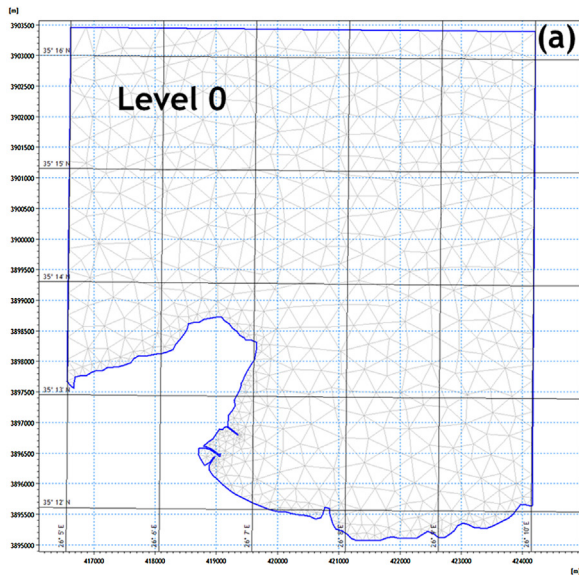


Figure 4 (a) Mesh with triangles for the outer model. (b) The bathymetry of the outer model domain.

flow and wave conditions, which in turn define the corresponding boundary conditions of the inmost level (i.e. level 2). The second, and more detailed, computational grid (level 2) extends in the longshore and cross-shore directions 1,400 m and 140 m, respectively, with maximum area of each triangular cell up to 1,050 m². The total number of grid cells in the inner domain is 2,135 with 1,282 nodes.

The bathymetry data of the inner model domain were digitized from maps of different spatial scales obtained from the Hellenic Navy Hydrographic Service (HNHS). The above data were enriched for the outer model domain with bathymetric grid points from the European Marine Observation and Data Network (EMODnet) Digital Bathymetry database with 1/8 of an arc minute (~230 m) resolution (Marine Information Service, 2016).

In Fig. 5(b), the 2D bathymetric representation of the study area is displayed in Google Earth for levels 1 and 2. The isobaths

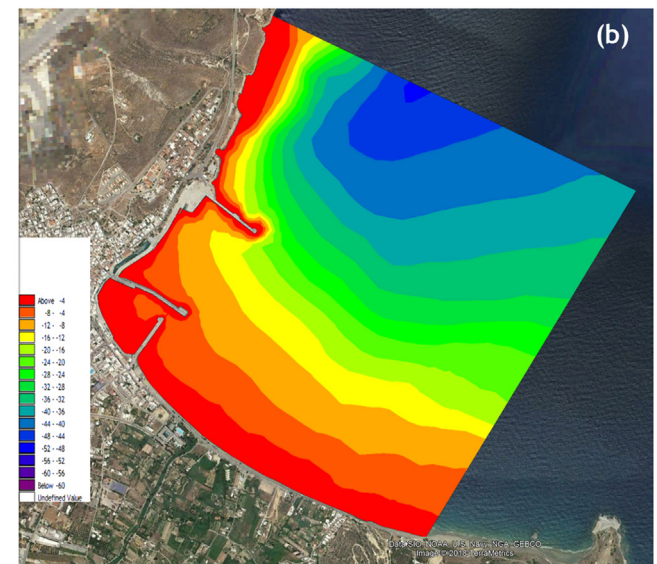
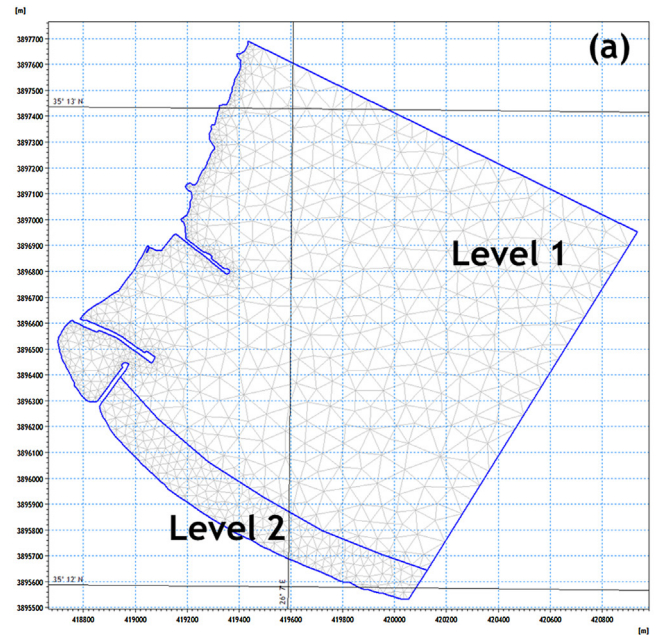


Figure 5 (a) Mesh with triangles using two levels for the inner model domain. (b) The inner model domain showing the bathymetry of the examined area.

from –20 m to lower depths are generally parallel to the shoreline and are evenly flattened going from the offshore part towards the shore. The highest depth (close to –50 m) is encountered in the north-western part of level 1 while the 10-m isobath is about 410 m from the coastline. In the eastern part of Sitia beach, there are beachrocks aligned parallel to the shoreline starting approximately from –1.5 m depth and ending to the coast. The formations act as natural submerged breakwaters mitigating erosion phenomena at this part of the coast.

4.2. Wave conditions

As regards the wave characteristics of the wider study area, the analysis is relied on 1-year time series, between 01/01/

2016 and 31/12/2016, at the middle point of the boundary of the outer model, i.e. at P_{out2} (see also Fig. 3, left map), with geographical coordinates 35.271°N – 26.125°E , obtained from the Mediterranean Sea Waves database. The relevant information include significant wave height H_S , peak wave period T_P and mean wave direction θ_m (measured clockwise from north), with an 1-hour resolution. These time series were used as input for the wave propagation from the offshore to the near-shore using MIKE21 CFM (SW and HD modules). After this simulation, the spectral time series were extracted for the northern and eastern boundaries of the inner model domain (with the finest triangular elements), presented in the right map of Fig. 3, in order to be used as input for the rest simulations.

The basic statistical measures at P_{out2} include mean value (m), standard deviation (sd), minimum (min) and maximum (max) values, 50th percentile ($p50$), skewness (sk) and kurtosis (ku), and the results are presented in Table 1. On average, the wave intensity is characterized low with mean values $m_{H_S} = 0.9$ m, $m_{T_P} = 5.08$ s and $m_{\theta_m} = 394.1^{\circ}$. The most intense wave incident occurred on 6th February 2016 with $H_S = 4.8$ m and corresponding $T_P = 9.23$ s and $\theta_m = 344.4^{\circ}$ during a two-day storm. The value of sk_{T_P} (0.23), close to zero, indicates that the distribution of the corresponding data is close to be symmetrical while the highest value of ku (7.1) is given by H_S indicating a sharp peak of the distribution.

As regards θ_m , the low value of sd (0.6) corresponds to a circular dataset that is highly concentrated, which can be also verified in Fig. 6, while sk value close to zero (-0.01) denotes a unimodal distribution. The wave rose of H_S at P_{out2} is depicted in Fig. 6, along with the corresponding frequencies of occurrence. The scattering of wave directions is limited to the sector $[285^{\circ}, 15^{\circ}]$ due to the topography and coast orientation of the study area with the prevailing wave directions coming from the north direction (sector $[300^{\circ}, 315^{\circ}]$), which are attributed to the very large fetch (390 km). The highest frequency of occurrence (13%) as regards wave propagation in the dominant direction is observed for values of H_S between 0.5 m and 1 m while the corresponding values of T_P exhibiting the highest frequency of occurrence are between 4 s and 6 s. Intense sea states ($H_S > 2.5$ m) with the highest frequency of occurrence (2%) correspond to the sector $[345^{\circ}, 0^{\circ}]$.

4.3. Input data

For practical reasons, the period of the simulation is confined to one year, i.e. from January 1 to December 31, 2016. As already mentioned the bathymetry resolution for the inner model domain gets progressively finer as we move from level 1 to level 2, which is the area of interest as concerns the simulation results and the evaluation of the methodology.

The timestep is set to $\Delta t = 3600$ s, equal with the time interval of the available time series. Prior to the description of the input data for the one-year wave time series, let it be mentioned that the authors kept some parameters at their default values since no in situ measurements were available for calibration of the model.

As regards HD module, the most essential input data include: wave radiation stress gradients that force the flows, bed resistance, eddy viscosity and boundary conditions. Eddy viscosity is based on the Smagorinsky coefficient with a constant value at 0.28, bed resistance expressed through the Manning number was fixed ($32 \text{ m}^{1/3}/\text{s}$) in the entire inner model domain apart from its south-eastern part due to the presence of bedrock formations while density is not updated during the simulation (barotropic mode). Let us note that tidal potential is very low in Sitia Bay thus it is not considered in the model setup. At the open boundaries, current velocities (varying in time and along boundary) are used as input obtained from the simulation results of the outer model while at the closed boundary, the normal velocity component is set to zero, assuming full slip boundary conditions.

As in the HD module, the instationary mode as regards time formulation was adopted in the SW module as well, with a directionally decoupled parametric formulation. The conditions at the open boundaries (at the north and east side of the model domain) were kept constant in space (along the boundary line) and varying in time while the boundary data consisted of significant wave height H_S , peak wave period T_P , mean wave direction θ_m and directional spreading index n . Additional model parameters were wave breaking specified by the gamma parameter $\gamma_{wb} = 0.8$ constant in space, bottom friction specified by the Nikurdase roughness K_N , which was varying in space ranging from 6.25 mm to 0.25 for level 1, and 1.9 mm for level 2 while for the bedrock formations the value of 62.5 mm was selected.

Regarding the setting up of the ST module, sediment transport rates and bed level changes under the combined action of waves and currents are calculated through interpolation of sediment transport tables. These tables are generated in advance and include the following parameters: root-mean square wave height, peak period, current speed, wave height-to-water depth ratio, angle between current and waves, median grain diameter d_{50} and sediment grading. The ST calculations are activated at the initial th timestep while the timestep factor is set to 1, meaning that sediment transport rates and bed level are calculated every timestep. Apart from the flow (HD) and wave (SW) forcings, the specification of sediment properties and the considerations of morphological impact on hydrodynamics are two important features that need to be provided for the area of interest. To this end, as regards the granulometric composition of the bottom sediments in the study area, the sea bottom consists

Table 1 Basic statistics of the wave parameters obtained from the spectral time series at P_{out2} between 01/2016 and 12/2016. Square brackets denote units of the corresponding wave parameter where necessary.

	N	m	sd	min	$p50$	max	sk	ku
H_S [m]	8784	0.9	0.7	0.1	0.7	4.8	1.8 [–]	7.1 [–]
T_P [s]		5.08	1.53	1.37	5.21	10.15	0.23 [–]	2.9 [–]
θ_m [$^{\circ}$]		394.1	0.6 [–]	–	396.7	–	-0.01 [–]	0.7 [–]

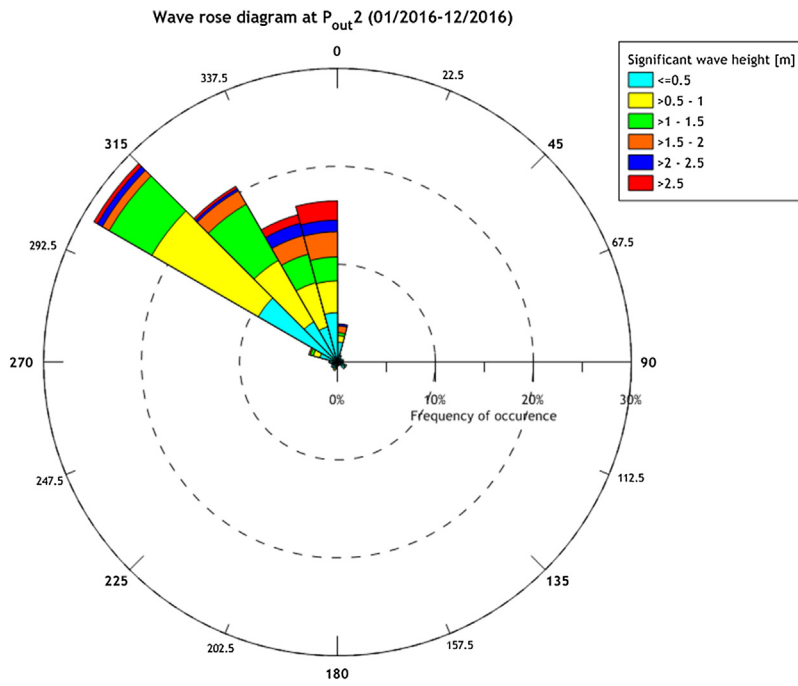


Figure 6 Rose diagram of significant wave height and wave direction at $P_{out,2}$ for the period 01/2016–12/2016. Intervals for H_S and θ_m are $\Delta H_S = 0.5$ m and $\Delta \theta_m = 15^\circ$, respectively.

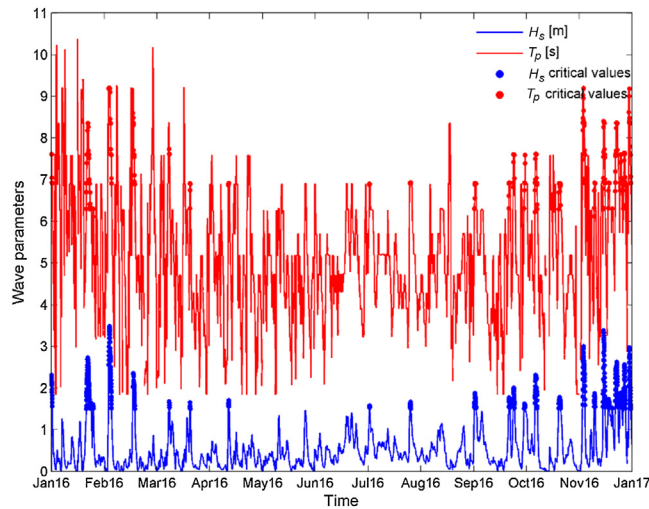


Figure 7 Time series of H_S and T_P at $P_{inn,m}$ for the year 2016. Blue and red dots indicate over-critical values of H_S and T_P , respectively.

of sand with an average diameter of d_{50} around 0.65–0.85 mm up to the isodepths of 1.5–2 m and with d_{50} between 0.08 mm and 0.25 mm for depths above 15 m (Anagnostou et al., 2017). Sediment grading was kept fixed, equal to 1.45, at the entire model domain. The initial bed layer thickness for all levels was set to 0.5 m apart from the bedrock part (0.0001 m).

In terms of the representative wave conditions (both over- and sub-critical ones), the parameters of the model setup remained the same except for the time formulation (quasi stationary mode) and the start time of the ST calculations

since all modules were synchronized to start at the same timestep.

5. Results

5.1. Representative wave conditions

In this work, the time period of the analyzed wave data is confined between 01/2016 and 12/2016; henceforth, when

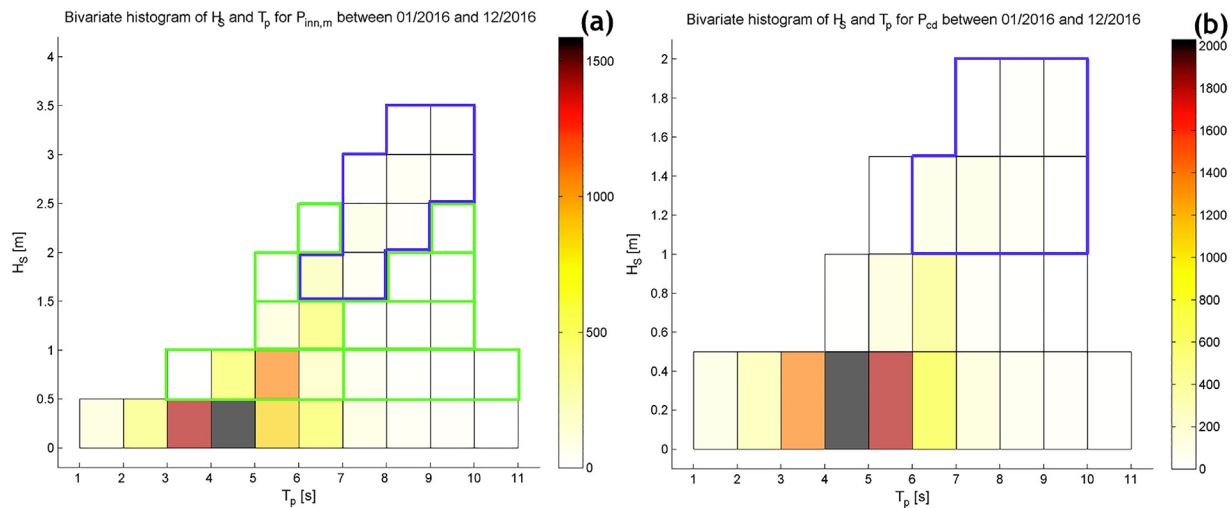


Figure 8 Bivariate histogram of (H_S, T_P) for (a) $P_{inn,m}$, and (b) P_{cd} for the year 2016. The blue closed polygon indicates the over-critical values and the green rectangles indicate the sub-critical pairs.

Table 2 Name of location, geographical coordinates, depth and distance from shore for the examined locations.

Location	Geographical coordinates (long., lat.) [°]	Depth [m]	Distance from shore [m]
A	(26.1090°, 35.2060°)	−1.23	26
B	(26.1101°, 35.2050°)	−1.42	38
C	(26.1113°, 35.2041°)	−1.38	37
D	(26.1129°, 35.2030°)	−1.08	37
E	(26.1143°, 35.2024°)	−1.57	41
F	(26.1158°, 35.2017°)	−1.02	39
G	(26.1172°, 35.2013°)	−0.87	40
H	(26.1188°, 35.2007°)	−0.58	45

we refer to the full time series of 2016 we use the term “reference wave data”. The time series of the reference wave data for H_S and T_P at $P_{inn,m}$ is presented in Fig. 7. Consecutive intense wave conditions, with H_S above 1.5 m, occurred mainly during the last two months of the examined year. In the majority of the timesteps, high values of H_S correspond to high values of T_P as regards the examined location, rendering these pairs candidates for the initiation motion of sediments. According to the methodology, the first step is to calculate representative orbital velocity, bed shear stress and wave shear velocity by using the H_S and T_P time series of P_{cd} by applying Eqs. (4), (5) and (8), respectively. Based on the calculation of the Shields parameter and its threshold value, the over-critical wave conditions at P_{cd} are determined. Classifying the reference wave data at P_{cd} into classes of H_S and T_P with intervals 0.5 m and 1 s, respectively, we obtain Fig. 8(b). From this figure it can be noticed that the lower threshold values for the onset of sediment transport, based on the Shields criterion, correspond to waves higher than 1 m with peak period between 6 s and 10 s and mean wave direction around 25°–29° as regards P_{cd} .

Identifying the corresponding wave conditions at the boundary of the inner model, i.e. at $P_{inn,m}$, the corresponding threshold values are presented in Fig. 8(a) with the blue outline having minimum values 1.5 m and 6 s for H_S and T_P respectively, and in the range [355°, 5°] for θ_m . As a whole,

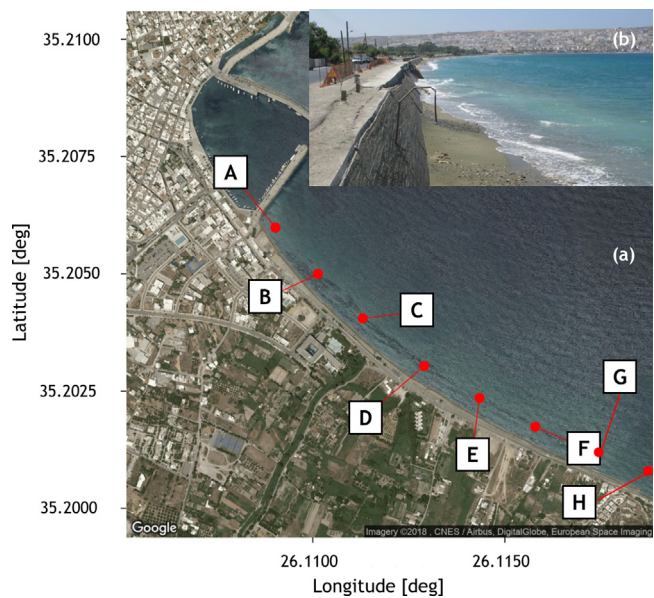


Figure 9 (a) Map of the examined area (from Google Earth) indicating the locations for the estimation of bed level based on the proposed methodology at Sitia beach. (b) Photo near location G indicating erosion problem.

nine representative intense wave conditions (i.e. over-critical pairs) were taken into account for the estimation of rates of bed level change over the examined period. From the same figure, the calm (sub-critical) wave conditions were derived by further grouping these classes into eight representative calm wave conditions with the same interval for H_S and a varying one for T_P , depending on the bivariate histogram. Let us remind that small values of H_S (i.e. <0.5 m) are not considered in the next steps of the technique since the model runs of the sensitivity analysis, performed by the same authors, demonstrated that such waves present almost negligible quantities of sediment transport rates. Altogether, 17 (H_S , T_P) pairs, along with the corresponding values of θ_m , are considered in the analysis, which were simulated separately.

5.2. Application of the methodology at the examined coast

Eight shallow locations are selected for examining the methodology described in Section 2; their geographical location, depth and distance from shore are given in Table 2. These points cover a distance of approximately 1,100 m along the coast with their in-between distance being around 150 m; their location on the map is shown in Fig. 9(a).

As regards the over-critical (H_S , T_P) pairs, the values of rates of bed level change for locations C, D, E, F, G and H are negative, with values between -0.003 m/day and -0.036 m/day. In general, the eastern locations (i.e. E, F, G and H) present the highest negative rates of bed level change while the western locations A and B are characterized by negative and positive rates of varying magnitude. With respect to the sub-critical (H_S , T_P) pairs, smaller, negative and positive, rates of bed level change are provided by all locations compared to the above pairs with the highest positive value (0.034 m/day) encountered at location E and the highest negative value (-0.033 m/day) at location F.

A more analytic representation for estimating bed level with the proposed methodology is given in Fig. 10 for location A, and in Fig. 11 for location F regarding specific representative (H_S , T_P) pairs. At the left panels of the above figures, the vertical lines denote the time windows of the over-critical (H_S , T_P) pairs in terms of sediment initiation; in the examined annual time scale, 30 time frames were identified by the methodology. At the right panels of the same figures, the rates of bed level change are plotted for the two different types of representative wave conditions (i.e. over- and sub-critical). As it was expected, the rates of bed level change for the over-critical (H_S , T_P) pair present higher values compared with the sub-critical pairs at both locations.

Specifically, as regards location A, the pattern of the over-critical wave case shows some resemblance with the sub-critical one; in both cases, the rate of bed level change strongly fluctuates during the 2-week simulation, taking mainly positive values, while at the 8th day of simulation a relative stabilization is evident. On the other hand, for location F, the rates present a dissimilar behaviour from location A; the rate of bed level change seems to be stabilized around zero after eight days of simulation for the over-critical representative wave conditions while it takes constantly negative values, after the second day of simulation, with bigger fluctuations for the sub-critical ones.

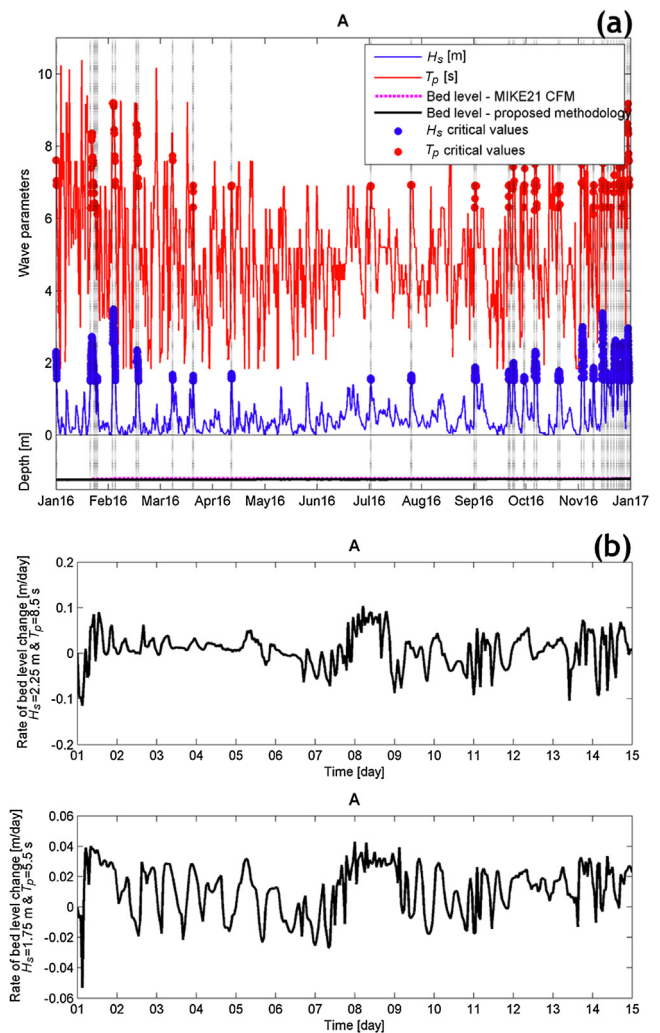


Figure 10 (a) Wave parameters along with bed levels obtained from the two approaches. (b) Rates of bed level change obtained from the proposed methodology for one over-critical and one sub-critical representative wave condition at point A.

In Fig. 12, the values of bed level obtained from the simulations results of MIKE21 CFM with the reference wave data as input, represented by the dashed line, and the proposed methodology, represented by the solid line, are plotted at the examined locations. From this figure, the following comments can be summarized:

- Locations B and D exhibit a very good agreement between the two approaches; throughout the year, the corresponding bed levels follow the same tendency and are very close with each other while as regards the last month, the deviation between the two bed level values is 0.7 cm and 0.4 cm, respectively, which are the smallest differences among the examined cases.
- Locations A and C, which follow a bathymetric profile with smooth to intermediate slopes (not shown here), and location H as well, exhibit medium-size deviations at the end of 2016, with values between 2.2 cm and 2.8 cm, respectively; however, the resemblance of the pattern that the two lines follow throughout the year is rather poor.

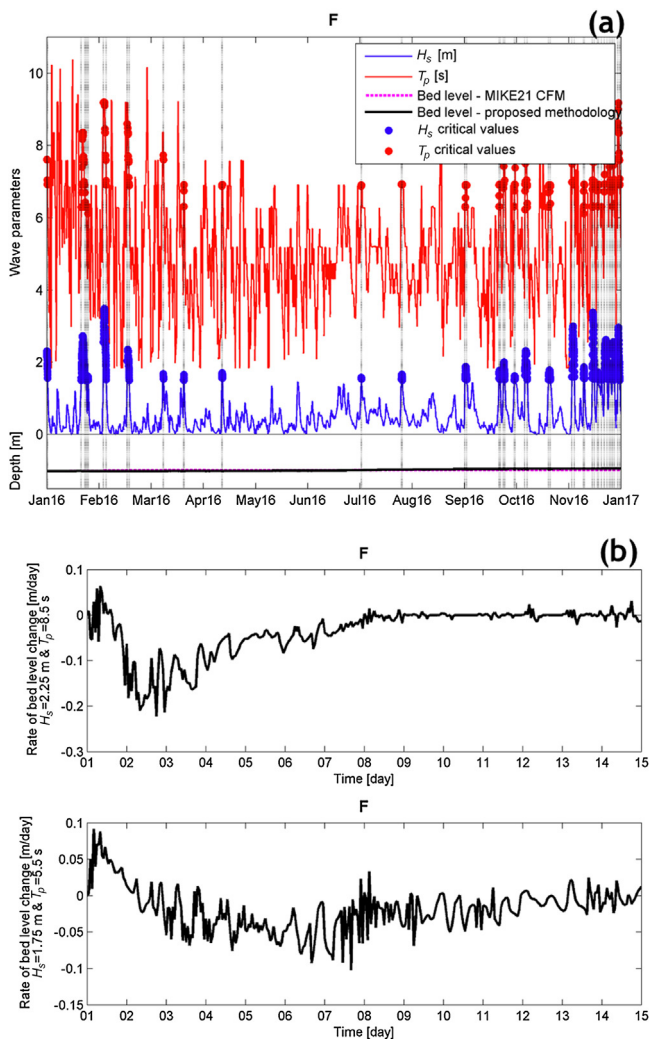


Figure 11 (a) Wave parameters along with bed levels obtained from the two approaches. (b) Rates of bed level change obtained from the proposed methodology for one over-critical and one sub-critical representative wave condition at point F.

- The locations E and F, with the latter having a steep bathymetric profile, exhibit the second largest deviation at the end of 2016 (4.5 cm) but the lines indicating the bed levels are in accordance in terms of the trend.
- Location G (see also Fig. 9(b)) presents the highest deviation (6.6 cm) compared with the reference time series.
- The bed level slope at locations A, B and C is positive indicating accretion in the western side of the Sitia coast while location D is characterized by a small negative slope (i.e. erosion pattern). Locations E and F present a steeper positive slope than the western locations, and locations G and H exhibit a higher negative slope than location D, implying more distinct erosion patterns. Overall, this behaviour coincides quite satisfactorily with the real situation encountered in the Sitia coast during the examined period, where the eastern part has been eroded to a

great extent leading to the collapse of the retaining wall of the coastal road.

6. Discussion

The scope of this work was to reduce the reference wave data (of one-year duration) into two groups, i.e. (i) the over-critical (H_S , T_P) pairs that fulfil the Shields criterion leading to sediment initiation, and (ii) the sub-critical (H_S , T_P) pairs that do not fulfil this criterion, in order to significantly reduce computational times and compare the estimated bed level values with the full case. The results of the proposed methodology compared to the ones obtained from utilizing the entire time series of the available wave data present similar trends, and the differences remain under 7%.

In this connection, some notable aspects should be remarked. Various sources of uncertainties as regards the discrepancies can be attributed to the assumptions that are imposed throughout the adopted technique. For instance, turbulence caused by wave breaking is not considered although it can be a source of sediment mobilization. Other uncertainties deal with the calculation of bottom orbital velocity, related indirectly with the Shields criterion, that does not take into account the presence of currents while the assumed spectral form might also influence bottom orbital velocity. For more details in terms of the potential sources of error in the calculation of bottom orbital velocity from wave spectral parameters such as H_S and T_P , see further assumptions provided by [Wiberg and Sherwood \(2008\)](#). Furthermore, in the context of the sensitivity analysis, the authors followed an alternative way to estimate bottom orbital velocity and friction factor. The corresponding values derived from the simulation results of the reference wave data reached common over-critical combinations of H_S and T_P .

Another potential source of uncertainty could be the estimation method of the mean rates of bed level change. Many dissimilar ways were tested by the authors including mean rates from one week, different mean rates based on the (H_S , T_P) pairs and the examined location, mean rates calculated with a smaller time interval during the simulation runs etc. However, the adopted approach showed consistently better performance in terms of bed level prediction.

Let us also highlight that a more proper and fair comparison would be to assess both results from model simulations with in situ measurements of bed level at the site of interest. The absence of real measurements has a twofold effect: (i) it places the comparison into relative terms, and (ii) it renders model calibration infeasible, thus the model results per se should be used with caution. Nevertheless, such comparison is beyond the scopes of this study. Moreover, due to the lack of real measurements, it is also recommended not to apply speed-up techniques since they require careful calibration and validation.

Another worth-mentioning fact refers to the distribution of wave direction. Specifically, the range of wave directions that affect significantly the morphological (bed level) conditions of the examined beach is very narrow since in the majority northern wave directions are dominant. This feature along with the gentle bottom slope and the uniformity of the coast as regards its shape render the study area a simple and easy example to implement this methodology compared to more complex cases.

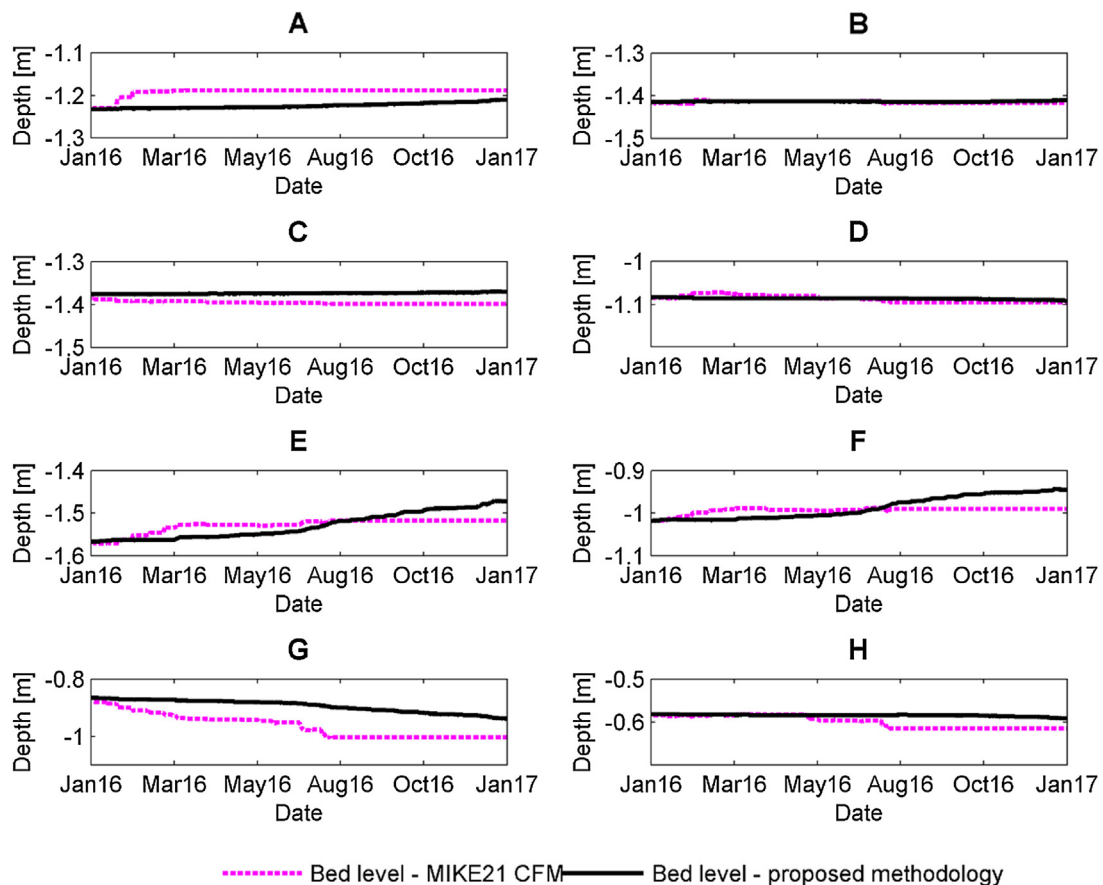


Figure 12 Bed levels derived from MIKE21 CFM (dashed red line) and the proposed methodology (solid black line).

In reference with the overall computation time of the model simulations, there is a striking discrepancy between the two approaches. For MIKE21 CFM with the full reference wave data as input, the total runtime was 542 h while for the 17 representative wave cases of the proposed methodology, the corresponding runtime was 2 h. Let us note that all simulations were conducted on an i7-2600 CPU server with 16 GB RAM and 3.40 GHz processor. Although current version of DHI is designed for parallel computing using graphics processors and could significantly accelerate the calculation process, still the present approach contributes to a significant runtime reduction, which for the particular non-parallel computing setup used is of the order of 99.6%. The latter result is quite impressive compared to the outcome presented in Fig. 12, at least for the case-study examined, characterised by mild bottom topography and coastal characteristics, and regularly in the distribution of offshore wave directions.

7. Conclusions

A cost-effective methodology is introduced to estimate long-term effects of waves represented by specific pairs of wave characteristics instead of the full wave time series, which is very demanding as regards computational cost. The proposed method is relatively easy to be applied and input reduction consists in defining the representative wave classes through

(H_s, T_p) pairs with reference to the Shields parameter criterion. A number of 17 representative wave conditions were derived from the reference wave data of the available time series with one-year duration. From the moment the over-critical wave conditions are found, the sub-critical wave classes can also be identified along with the corresponding frequency of occurrence; in this way, the full time series of wave height, period and direction can be appropriately classified into representative wave conditions. Having these triplets to hand, the dynamic coupled current-wave modelling, including the interaction with sediment transport, for each representative condition provides the desirable rates of bed level change, from which the final bed level can be estimated.

Comparing the values of bed level from the representative wave conditions with those from the reference time series, there was a good agreement for the examined locations, with the differences remaining under 7% at eight selected locations along the examined coast. Moreover, the bed evolution tendencies of the proposed methodology at the examined locations conform with the outcome from the full wave time series and the situation encountered in reality. For this reason, the suggested technique can be considered as a useful tool for reducing considerably computational cost in particular.

The results from the present analysis verify the fact that both intense wave conditions and calm periods should be taken into account when bed level (or shoreline) evolution is

examined. However, the proposed method was applied to a wave-dominated coast in the Sitia Bay with a limited range of incoming wave directions. Consequently, further improvements and validations should be made in order to take into consideration additional factors that influence sediment transport and bed level, such as currents, and examine the methodology at more complex areas, where preferably in situ measurements are available. Moreover, the impacts of a finer resolution of the involved wave parameters during the discretization process and a longer reference time series can be also analyzed.

Acknowledgments

F. Karathanasi would like to thank the GIS section of HCMR for providing the digitized bathymetric data, and F. Gad for the fruitful conversations on the 2DH model. The authors are also thankful to Ch. Anagnostou for useful data and discussion concerning the examined site, E. Moussoulis from DHI-Greece for providing the software licence and for his prompt feedback to the raised questions as regards model configuration, and the two anonymous reviewers for their helpful comments that greatly improved this manuscript.

References

- Alexandrakis, G., Gkionis, G., Petrakis, S., Kozyrakos, G., Kampanis, N.A., 2015. Study for the Effective Management of the Erosion Problem, the Protection and Recasting of the Coastline and the Reduction of Incoming Wave Energy, in the Sitia City Beachfront, and Makri Gialos. Technical Report. Coastal & Marine Research Laboratory (CRL), Institute of Applied & Computational Mathematics – Foundation for Research and Technology, Heracleion, 115 pp. (in Greek).
- Anagnostou, C., Belibassakis, K., Karathanasi, F., 2017. Coastal erosion in the Sitia Crete Bay – rehabilitation of the coast based on nourishment techniques as an alternative to hard work interventions. In: 7th National Conference on Management and Improvement of Coastal Zones, 20–22 November, Athens, 421–430.
- Aouiche, I., Daoudi, L., Anthony, E.J., Sedrati, M., Harti, A., Ziane, E., 2016. The impact of storms in the morphodynamic evolution of a human-impacted semi-sheltered beach (Agadir Bay, Morocco). *J. Afr. Earth Sci.* 115, 32–47, <http://dx.doi.org/10.1016/j.jafrearsci.2015.12.011>.
- Belibassakis, K.A., Karathanasi, F.E., 2017. Modelling nearshore hydrodynamics and circulation under the impact of high waves at the coast of Varkiza in Saronic-Athens Gulf. *Oceanologia* 59 (3), 350–364, <http://dx.doi.org/10.1016/j.oceano.2017.04.001>.
- Benedet, L., Dobrochinski, J.P.F., Walstra, D.J.R., Klein, A.H.F., Ranasinghe, R., 2016. A morphological modeling study to compare different methods of wave climate schematization and evaluate strategies to reduce erosion losses from a beach nourishment project. *Coast. Eng.* 112, 69–86, <http://dx.doi.org/10.1016/j.coastaleng.2016.02.005>.
- Clementi, E., Pistoia, J., Delrosso, D., Mattia, G., Fratianni, C., Storto, A., Ciliberti, S., Lemieux, B., Fenu, E., Simoncelli, S., Drudi, M., Grandi, A., Padeletti, D., Di Pietro, P., Pinardi, N., 2017. A 1/24 degree resolution Mediterranean analysis and forecast modeling system for the Copernicus Marine Environment Monitoring Service. Extended abstract. In: 8th EuroGOOS Conference, Bergen, 27–28.
- Corbella, S., Stretch, D.D., 2012. Predicting coastal erosion trends using non-stationary statistics and process-based models. *Coast. Eng.* 70, 40–49, <http://dx.doi.org/10.1016/j.coastaleng.2012.06.004>.
- Daghigh, H., Khaniki, A.K., Bidokhti, A.A., Habibi, M., 2017. Prediction of bed ripple geometry under controlled wave conditions: wave-flume experiments and MIKE21 numerical simulations. *Indian J. Geo Mar. Sci.* 46 (3), 529–537, <http://nopr.niscair.res.in/handle/123456789/40808>.
- Davidson-Arnott, R., 2009. *Introduction to Coastal Processes and Geomorphology*. Cambridge Univ. Press, Cambridge, 442 pp.
- DHI, 2016. MIKE 21 & MIKE 3 Flow Model FM, Hydrodynamic and Transport. Scientific Documentation.
- Dubarbier, B., Castelle, B., Marieu, V., Ruessink, G., 2015. Process-based modeling of cross-shore sandbar behavior. *Coast. Eng.* 95, 35–50, <http://dx.doi.org/10.1016/j.coastaleng.2014.09.004>.
- Foteinis, S., Synolakis, C.E., 2015. Beach erosion threatens Minoan beaches: a case study of coastal retreat in Crete. *Shore Beach* 83 (1), 53–62.
- Fredsøe, J., Deigaard, R., 1992. *Mechanics of Coastal Sediment Transport*. World Scientific, Singapore, 369 pp.
- Günther, H., Behrens, A., 2012. *The WAM model. Validation document Version 4.5.4*. Institute of Coastal Research Helmholtz-Zentrum Geesthach (HZG), 92 pp.
- Gad, F.K., Hatiris, G.A., Loukaidi, V., Dimitriadou, S., Drakopoulou, P., Sioulas, A., Kapsimalis, V., 2018. Long-term shoreline displacements and coastal morphodynamic pattern of North Rhodes Island, Greece. *Water* 10 (7), 849, <http://dx.doi.org/10.3390/w10070849>.
- Gharibreza, M., Nasrollahi, A., Afshar, A., Amini, A., Eisaei, H., 2018. Evolutionary trend of the Gorgan Bay (southeastern Caspian Sea) during and post the last Caspian Sea level rise. *Catena* 166, 339–348, <http://dx.doi.org/10.1016/j.catena.2018.04.016>.
- Hallermeier, R.J., 1980. Sand motion initiation by water-waves – 2 asymptotes. *J. Waterw. Port C. Div.* 106 (3), 299–318.
- Hallermeier, R.J., 1981. A profile zonation for seasonal sand beaches from wave climate. *Coast. Eng.* 4 (3), 253–277, [http://dx.doi.org/10.1016/0378-3839\(80\)90022-8](http://dx.doi.org/10.1016/0378-3839(80)90022-8).
- Hasselmann, K., Barnett, T.P., Bouws, E., Carlson, H., Cartwright, D.E., Enke, K., Ewing, J.A., Gienapp, H., Hasselmann, D.E., Kruseman, P., Meerburg, A., Müller, P., Olbers, D.J., Richter, K., Sell, W., Walden, H., 1973. Measurements of wind-wave growth and swell decay during the Joint North Sea Wave Project (JONSWAP). In: group, J. (Ed.), *Hydraulic Engineering Reports*. Deutsches Hydrographisches Institut, Hamburg, p. 95.
- Karathanasi, F., Belibassakis, K., Anagnostou, C., 2017. Simulation of wave field and sediment transport at the Sitia bay. In: 7th National Conference on Management and Improvement of Coastal Zones, 20–22 November, Athens, 33–42.
- Madsen, O.S., 1994. Spectral wave-current bottom boundary layer flows. In: *Coast. Eng.; Proceedings 24th International Conference Coastal Engineering Research Council, American Society of Civil Engineers, Kobe, Japan (1994)*, 384–398, <http://dx.doi.org/10.9753/icce.v24.p.384>.
- Marine Information Service, 2016. EMODnet Digital Bathymetry (DTM). Marine Information Service, <http://dx.doi.org/10.12770/c7b53704-999d-4721-b1a3-04ec60c87238>.
- Ortiz, A.C., Ashton, A.D., 2016. Exploring shoreface dynamics and a mechanistic explanation for a morphodynamic depth of closure. *J. Geophys. Res. Earth* 121 (2), 442–464, <http://dx.doi.org/10.1002/2015jf003699>.
- Ramakrishnan, R., Agrawal, R., Remya, P.G., NagaKumar, K.C.V., Demudu, G., Rajawat, A.S., Nair, B., Nageswara Rao, K., 2018. Modelling coastal erosion: a case study of Yarada beach near Visakhapatnam, east coast of India. *Ocean Coast. Manage.* 156, 239–248, <http://dx.doi.org/10.1016/j.ocecoaman.2017.08.013>.
- Ranasinghe, R., 2016. Assessing climate change impacts on open sandy coasts: a review. *Earth-Sci. Rev.* 160, 320–332, <http://dx.doi.org/10.1016/j.earscirev.2016.07.011>.

- Soulsby, R., 1997. *Dynamics of Marine Sands: A Manual for Practical Applications*. Thomas Telford Publications, London, 249 pp.
- Toimil, A., Losada, I.J., Camus, P., Díaz-Simal, P., 2017. Managing coastal erosion under climate change at the regional scale. *Coast. Eng.* 128, 106–122, <http://dx.doi.org/10.1016/j.coastaleng.2017.08.004>.
- Van Rijn, L.C., 1993. *Principles of Sediment Transport in Rivers, Estuaries and Coastal Seas*. Aqua Publications, Amsterdam, The Netherlands, 690 pp.
- Walstra, D.J.R., Hoekstra, R., Tonnon, P.K., Ruessink, B.G., 2013. Input reduction for long-term morphodynamic simulations in wave-dominated coastal settings. *Coast. Eng.* 77, 57–70, <http://dx.doi.org/10.1016/j.coastaleng.2013.02.001>.
- Wiberg, P.L., Sherwood, C.R., 2008. Calculating wave-generated bottom orbital velocities from surface-wave parameters. *Comput. Geosci.-UK* 34 (10), 1243–1262, <http://dx.doi.org/10.1016/j.cageo.2008.02.010>.